Effects of phytoplankton community on production, size and export of large aggregates: A world-ocean analysis

Lionel Guidi, Lars Stemmann, George A. Jackson, Frederic Ibanez, Hervé Claustre, Louis Legendre, Marc Picheral, Gabriel Gorsky

Limnol. Oceanogr., 54(6), 2009, 1951–1963

Effects of phytoplankton community on production, size and export of large aggregates: A world-ocean analysis

Lionel Guidi,[a,b,1,*] Lars Stemmann,[a,b] George A. Jackson,[c] Frédéric Ibanez,[a,b] Hervé Claustre,[a,b] Louis Legendre,[a,b] Marc Picheral,[a,b] and Gabriel Gorsky[a,b]

[a] Université Pierre et Marie Curie, Université Paris 06, Unité Mixte de Recherche 7093, Laboratoire d'Océanographie de Villefranche, Villefranche-sur-Mer, France

[b] Centre National de la Recherche Scientifique, Unité Mixte de Recherche 7093, Laboratoire d'Océanographie de Villefranche, Villefranche-sur-Mer, France

[c] Department of Oceanography, Texas A&M University, College Station, Texas

Abstract

We recorded vertical profiles of size distributions of large particles (>100 μm) to a 1000-m depth in the Atlantic, Indian, and Pacific Oceans and in the Mediterranean Sea with the Underwater Video Profiler. Of the 410 profiles used in our analysis, 193 also included temperature, salinity, and high-performance liquid chromatography (HPLC)-resolved pigments, which were used to characterize the size structure of the phytoplankton community. Classification analysis identified six clusters of vertical profiles of size distributions of particles. Each cluster was characterized by the size distribution of its particles in the mesopelagic layer and the change of the particle-size distribution with depth. Clusters with large particles in the mesopelagic layer corresponded to surface waters dominated by microphytoplankton, and those with small particles corresponded to surface waters dominated by picophytoplankton. We estimated the mass flux at 400 m using a relationship between particle size and mass flux. Principal-component regression analysis showed that 68% of the variance of the mass flux at 400 m was explained by the size structure of the phytoplankton community and integrated chlorophyll *a* in the euphotic zone. We found that coefficient *k* in the Martin power relationship, which describes the decrease in the vertical mass flux with depth, varies between 0.2 and 1.0 in the world ocean, and we provided an empirical relationship to derive *k* from the size structure of phytoplankton biomass in the euphotic zone. Biogeochemists and modelers could use that relationship to obtain a realistic description of the downward particle flux instead of using a constant *k* value as often done.

Factors that control carbon export to the deep ocean have received considerable attention during the last three decades. Organic matter is exported mainly by large, fast-sinking particles (Alldredge and Silver 1988). Sinking speed and vertical flux of particles (mostly aggregates) have been linked to the size of particles in many oceanic regions (Peterson et al. 2005; Guidi et al. 2008) or to their mineral content (i.e., the "ballast effect," Armstrong et al. 2002). Despite the importance of the particle size in organic matter export, global variations in particle abundance as a function of size are poorly known.

The size distributions of small particles (1 μm to 100 μm) have been characterized in the past (Sheldon et al. 1972), but the information on the horizontal and vertical variations in the size distributions of larger particles is scarce, even though large particles are responsible for a significant fraction of carbon transport to the deep ocean (Stemmann et al. 2002). The recent availability of imaging sensors and fast computers to analyze images have led to the development of in situ camera systems that have been used to record vertical profiles of size distribution and abundance of particles (Stemmann et al. 2002).

Carbon export from the euphotic zone has been related to new production in phytoplankton (Eppley and Peterson 1979). The flux of large particles has often been ascribed to microphytoplankton (>20 μm) in the euphotic zone, particularly diatoms (Smetacek 1985), and the polar ocean and coastal upwelling regions are examples of areas where this is believed to occur (Alldredge and Silver 1988). Smaller cells [i.e., picophytoplankton (<2 μm) and nanophytoplankton (2 μm to 20 μm)] can contribute to the downward carbon flux through food-web interactions (Gorsky et al. 1999; Olli et al. 2007). Oligotrophic regions, where small cells dominate phytoplankton production, play a significant role in the global carbon flux because they represent >50% of the global ocean area. In the equatorial Pacific Ocean, picoplankton are responsible for 87% of the particulate organic carbon (POC) export via detritus (Richardson and Jackson 2007). Hence, the size of phytoplankton is an important factor controlling the export and sequestration of atmospheric carbon in the ocean (Michaels and Silver 1988; Boyd and Newton 1999).

In this paper, we use an extensive data set of particle-size distributions that covers a wide range of trophic conditions in the ocean, from oligotrophy to eutrophy, to test the following three ideas: first, the variability in size distributions of large particles (>250 μm) in the world ocean shows spatio-temporal patterns; second, vertical mass fluxes of particles at depth can be calculated from observed size distributions of particles and the decrease of these fluxes

* Corresponding author: lionelg@hawaii.edu

[1] Present address: University of Hawaii, Department of Oceanography, Honolulu, Hawaii

Table 1. For each cruise, location, name, dates, numbers of vertical profiles of particle-size distribution corresponding to the six clusters identified by classification analysis (columns G_1 to G_6), and total number of profiles (rightmost column).

Location	Cruise	Start	End	G_1	G_2	G_3	G_4	G_5	G_6	Total
Aegean Sea	EGEE2	Mar 98	Mar 98	1	0	0	0	0	0	1
Atlantic O.	EUMELI5	Dec 92	Dec 92	0	0	0	0	5	3	8
Atlantic O.	MAINE2002	Sep 02	Sep 02	0	12	4	0	0	0	16
Atlantic O.	MARECO2002	Nov 02	Nov 02	10	0	0	0	0	0	10
Atlantic O.	MARECO2004	Jun 04	Jul 04	0	2	4	0	9	18	33
Atlantic O.	NOR2000	Mar 00	Mar 00	0	0	0	6	0	0	6
Atlantic O.	POMME1L1	Feb 01	Feb 01	0	1	15	12	0	0	28
Atlantic O.	POMME1L2	Mar 01	Mar 01	0	4	0	19	0	0	23
Atlantic O.	POMME2L1	Mar 01	Apr 01	0	2	24	12	2	0	40
Atlantic O.	POMME3L1	Aug 01	Aug 01	0	1	2	0	0	0	3
Atlantic O.	POMME3L2	Sep 01	Oct 01	0	1	15	0	7	0	23
Indian O.	ANTARES3	Oct 95	Oct 95	0	0	3	0	9	0	12
Indian O.	KEOPS	Jan 05	Feb 05	0	0	1	0	0	5	6
Indian O.	SS052006	May 06	May 06	3	13	4	10	0	0	30
Mediterr. Sea	ALMOFRONT1L2	Mar 03	Jun 03	0	3	1	0	1	5	10
Mediterr. Sea	BARMED	Nov 95	Dec 95	1	4	4	0	0	2	11
Mediterr. Sea	DYFABAC	May 95	May 95	0	1	4	0	0	0	5
Mediterr. Sea	DYNAPROC	May 91	May 91	0	9	2	0	5	0	16
Mediterr. Sea	EUROMARGE	Jun 95	Jun 95	0	3	2	0	0	1	6
Mediterr. Sea	FRONTAL93	Jan 93	Dec 93	0	4	1	0	3	1	9
Mediterr. Sea	FRONTAL94	Jan 94	Dec 94	1	9	5	1	8	4	28
Mediterr. Sea	FRONTAL95	Jan 95	Mar 95	0	0	1	0	3	7	11
Mediterr. Sea	FRONTAL96	Feb 96	Jun 96	0	0	3	2	1	1	7
Mediterr. Sea	PAULINE	Nov 94	Nov 94	0	0	0	0	1	0	1
Mediterr. Sea	PICNIC	Mar 95	Mar 95	0	0	0	0	0	1	1
Pacific O.	BIOSOPE	Oct 04	Dec 04	11	9	20	0	11	15	66
Total				27	78	115	62	65	63	410

with depth occurs as described by the Martin power relationship; third, these fluxes and the values of the k parameter in the Martin relationship are related to characteristics of phytoplankton in surface waters.

Methods

Data on particles—Using three generations of the Underwater Video Profiler (UVP, Laboratoire d'Océanographie Biologique et d'Ecologie du Plancton Marin), we sampled particle-size distributions between the surface and 1000-m depth throughout the world ocean during the last two decades (Table 1). The UVP records images of particles illuminated in slabs of water that have well-defined volumes ranging from 0.20 liters to 10 liters, depending on the UVP generation. At sea, the UVP is lowered at a speed of 1 m s^{-1}, which is fast enough to avoid overlapping image regions. The analysis of images provides quantitative information on the sizes and shapes of objects in the field of vision of the UVP that can be used to calculate the distributions of particle sizes and the abundances of large plankton organisms (Gorsky et al. 2000; Stemmann et al. 2008). The minimum diameter of detectable particles has decreased from 250 μm to 90 μm over the three instrument generations; the effective maximum particle diameter depends on the sample volume and the particle concentration (McCave 1984; Jackson et al. 1997). The pictures are recorded digitally and processed by image-analysis software to assign a projected area to each particle. The equivalent spherical diameter (ESD) is calculated assuming that the projected area is a circle. The instruments have been calibrated in a seawater tank using natural particles corresponding to different types of aggregates to determine a conversion from pixels to metric units (Gorsky et al. 2000; Stemmann et al. 2002). The three generations of the instrument have been inter-calibrated, and the consistency of measurements has been checked (Guidi et al. 2007).

Vertical profiles were recorded using the UVP on 27 different cruises in the Pacific, Atlantic, and Indian Oceans, and in the Mediterranean Sea for more than 1300 deployments. The profiles of particle-size distributions were assembled into a single database. In this study, we restricted the diameter of interest to a range of 250 μm to 1.5 mm in order to be able to use the data from all three UVP generations. For reasons explained next, the present study considers only 410 of the available 1300 profiles. We calculated particle-size distributions by averaging particle concentrations over 5-m depth intervals.

In order to minimize extraneous effects on particle distributions, we selected 410 profiles from the 1300 available. The subset consisted of profiles recorded in relatively vertically homogeneous water masses, at stations where water depth was $\geq$1300 m, and for which there was no evidence of light effects on the UVP measurements deeper than 20 m. The vertical homogeneity of the water masses was checked by visual examination of the temperature–salinity (TS) profiles. We removed profiles that showed sharp variation of particle abundance with depth,

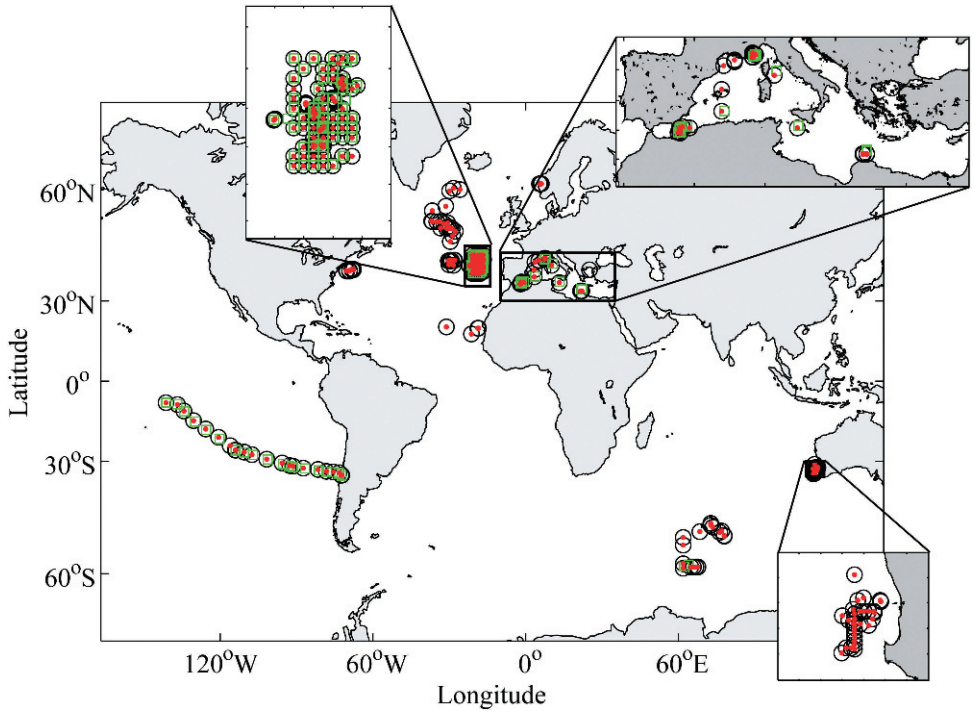

Fig. 1. Locations of the vertical profiles of UVP (black circles), CTD (red dots), and pigments (green squares) in the world ocean.

which probably indicated lateral transport in intermediate nepheloid layers or high shear rate generated by strong currents. Profiles with abnormally high concentrations of particles near the surface, which was indicative of contamination by light, were also removed. Each of the 410 selected profiles had a vertical resolution of 5 m, from 20 m to 1000 m (Table 1).

Ancillary data—During some UVP deployments, TS profiles were recorded with a conductivity–temperature–depth (CTD) profiler (SeaBird SBE911), and water samples were collected with Niskin bottles mounted on a rosette and filtered onto glass-microfibre filters (grade GF/F, Whatman) for phytoplankton pigment determination. We used the TS profiles to calculate the mixed-layer depth (MLD) as the depth at which density was 0.01 kg m^{-3} larger than at 1 m. We assumed that the UVP and water-property data had been sampled at the same location when they had been collected, within 0.1° latitude and 0.1° longitude in space and within 1 d in time of each other. Some 193 of the 410 profiles provided UVP, TS, and pigment data (Fig. 1).

Pigment determination was performed using high-performance liquid chromatography (HPLC) techniques described in Vidussi et al. (1996) for all cruises, except for ALMOFRONT1, BIOSOPE, and KEOPS, where pigments were analyzed according to Mantoura and Llewellyn (1983) and Ras et al. (2008).

We used the method proposed by Claustre (1994) and further improved by Uitz et al. (2006) to estimate the contribution of three pigment-based size classes (microplankton, nanoplankton, and picophytoplankton; f_{micro}, f_{nano}, and f_{pico}, respectively) to the total phytoplankton biomass. Briefly, this method (detailed in Uitz et al. 2006) takes into consideration seven diagnostic pigments representative of the major phytoplankton taxa [i.e., fucoxanthin (Fuco), peridinin (Peri), 19′-hexanoyloxyfucoxanthin (19′-HF), 19′-butanoyloxyfucoxanthin (19′-BF), alloxanthin (Allo), zeaxanthin (Zea), and total chlorophyll *b* (TChl *b*), here defined as the sum of chlorophyll *b* and divinyl-chlorophyll *b*] to compute the fractions of three pigment-based size classes with the following empirical equations (notation summarized in Table 2):

$$f_{micro} = (1.41\text{Fuco} + 1.41\text{Peri})/\text{wDP} \quad (1a)$$

$$f_{nano} = (0.60\text{Allo} + 0.3519'\text{BF} + 1.2719'\text{HF})/\text{wDP} \quad (1b)$$

$$f_{pico} = (0.86\text{Zea} + 1.01\text{TChl } b)/\text{wDP} \quad (1c)$$

where wDP is the weighted sum of these concentrations:

$$\text{wDP} = 1.41\text{Fuco} + 1.41\text{Peri} + 0.60\text{Allo} + 0.3519'\text{BF} + 1.2719'\text{HF} + 0.86\text{Zea} + 1.01\text{Tchl } b \quad (2)$$

Total chlorophyll *a* (TChl *a*) is the sum of chlorophyll *a* + divinyl-chlorophyll *a* concentrations. Total chlorophyll concentration (B_a) was calculated by integrating TChl *a* over the euphotic zone. The biomass associated with each phytoplankton group was computed as

Table 2. Symbols, descriptions, and dimensions (M for mass, L for length, T for time) of the variables and parameters used in the present paper.

Symbol	Description	Dimension
Particle data and related equations		
a	Constant coefficient (Eq. 5): Junge-type distribution	L^{-4+k}
b	Constant exponent (Eq. 5): Junge-type distribution	—
d	Particle diameter	L
C_1, C_2, C_4	Components of the PCR analysis	—
F	Generic mass flux	$M\ L^{-2}\ T^{-1}$
F_{100}	Mass flux at 100 m (Martin et al. 1987)	$M\ L^{-2}\ T^{-1}$
F_{400}	Size-spectral estimate of mass flux at 400 m	$M\ L^{-2}\ T^{-1}$
F_z	Mass flux at depth z (Martin et al. 1987)	$M\ L^{-2}\ T^{-1}$
k	Exponent of the Martin power relationship	—
m	Particle mass	M
n	Particle number spectrum	L^{-4}
V	Volume of a particle	L^3
w	Particle sinking speed	$L\ T^{-1}$
x_i	UVP minimum particle diameter	L
x_s	UVP maximum particle diameter	L
z	Depth	L
Z_e	Depth of the euphotic zone	L
ΔC	Concentration of particles	L^{-3}
Δd	Particle diameter range	L
Δs	Generic for particle size range	L
HPLC pigment data and related equations		
19′-BF	19′-butanoyloxyfucoxanthin	$M\ L^{-3}$
19′-HF	19′-hexanoyloxyfucoxanthin	$M\ L^{-3}$
Allo	Alloxanthin	$M\ L^{-3}$
B_a	Total chlorophyll concentration	$M\ L^{-2}$
B_{micro}, B_{nano}, B_{pico}	Biomass of micro-, nano-, pico-phytoplankton	$M\ L^{-2}$
f_{micro}, f_{nano}, f_{pico}	Fraction of micro-, nano-, pico-phytoplankton	—
Fuco	Fucoxanthin	$M\ L^{-3}$
Peri	Peridinin	$M\ L^{-3}$
TChl a	Total chlorophyll a	$M\ L^{-3}$
TChl b	Total chlorophyll b	$M\ L^{-3}$
wDP	Weighted sum of pigment concentrations	$M\ L^{-3}$
Zea	Zeaxanthin	$M\ L^{-3}$

$$B_{micro} = f_{micro} B_a \tag{3a}$$

$$B_{nano} = f_{nano} B_a \tag{3b}$$

$$B_{pico} = f_{pico} B_a \tag{3c}$$

The euphotic zone was assumed to extend downward to the 1% surface irradiance level, and its depth (Z_e) was calculated from the vertical profiles of Tchl a according to Morel and Maritorena (2001) using the iterative process described in Morel and Berthon (1989).

Treatment of size distributions of particles—The size spectrum of particles [$n(s) = n$] is usually calculated in terms of the concentration (number per unit volume) of particles (ΔC) in a given size range (Δs):

$$n = \Delta C / \Delta s \tag{4}$$

Although any measure of particle size can be used for s, the particle diameter (d) is used in this study.

Segments of the particle-size spectrum frequently fit an expression of the form

$$n = a d^b \tag{5}$$

where a and b are constants (Sheldon et al. 1972; McCave 1984; Jackson et al. 1997). The slope of the Junge-type particle-size spectrum is often calculated from $\ln(n) = \ln(a) + b \ln(d)$, where ln stands for natural logarithm. The slope (b) is used as the descriptor of the particle-size distribution in this study. For example, $b = -5$ indicates a large proportion of smaller particles present, whereas $b = -3$ indicates a preponderance of large particles.

All vertical profiles of slopes were smoothed by the eigenvector filtering method (EVF) in order to remove spikes associated with small-scale vertical variability (Vautard and Ghil 1989; Ibanez and Etienne 1992). The EVF procedure corresponds to a principal-component analysis (PCA) calculated on the autocovariance matrix of the slopes of the original data profile. The first and second axes extracted from the PCA represent the main modes of variability of the vertical distribution of b. The smoothing window was determined for each profile using its autocorrelation function.

Assuming that the mass $m(d)$ and sinking speed $w(d)$ of individual particles are functions of d, then the total mass of particles in the size range Δd is $n(d)m(d)\ \Delta d$, and the mass flux in that interval is $n(d)m(d)w(d)\ \Delta d$ (Guidi et al. 2008). The sinking speed of a particle depends on both its diameter and its mass. The mass depends on the constituents making up the particles. Here, we assume that all particles are composed of similar constituents such that the mass depends only on the particle size. This assumption is reasonable knowing that a global relationship exists between particle-size distribution and particle flux (Guidi et al. 2008). The relationship would not hold if mass and settling speed were independent of diameter. The authors concluded that particle-size distribution can be used as an estimator of particle flux. The total mass flux (F) is then the integral of the size-dependent mass flux (Guidi et al. 2008):

$$F(d) = \int_{x_i}^{x_s} n(d)m(d)w(d)\ \Delta d \tag{6}$$

In practice, particle mass and particle weight are often described using relationships of the form $m = yd^x$ or $w = yd^x$, where y and x are obtained by fitting the relationship to data that usually come from the surface layer. Note that if both $w(d)$ and $m(d)$ are given by power relationships, then so is the resulting combined quantity:

$$w \cdot m = A \cdot d^B \tag{7}$$

Guidi et al. (2008) used 108 pairs of sediment-trap data and particle-size distribution data to estimate the values of the

two constants in Eq. 7, and they obtained $A = 109.5$ and $B = 3.52$.

In order to estimate the total particle flux, Eq. 6 should be integrated over the entire size range of particles (i.e., 0 to maximum size). In the present study, where the available size range is 250 μm (x_i) to 1.5 mm (x_s), the mass flux was calculated over that range (Eq. 6). A sensitivity analysis was conducted to estimate the difference between flux estimates using the largest common size range for all UVP generations (i.e., 250 μm to 1.5 mm) and the largest size range available only for the latest UVP generation (i.e., 90 μm to 2 cm). The maximum ratio between the two flux estimates was two. Given that the vertical fluxes in the global ocean vary by three orders of magnitude, the possible error associated with using the smallest common size range to the three UVP generations is relatively small (Guidi et al. 2008).

Vertical profiles of total particle fluxes were calculated from the profiles of particle-size distributions using Eq. 6. The decrease of the estimated flux with depth was modeled by fitting a power law function to the data. That function is known as the Martin power relationship (Martin et al. 1987):

$$F_z = F_{100}(z/100)^{-k} \quad (8)$$

where z is the depth and k is the rate at which the flux measured at 100 m decreases with depth. In other words, the higher the value of k, the higher the rate at which the flux decreases.

Relationships between k and the fractions of microplankton and picophytoplankton (f_{micro} and f_{pico}) in the water column above Z_e were examined using Spearman's correlations and linear regressions. A possible seasonal effect on k was tested using Kruskal-Wallis nonparametric one-way analysis of variance (ANOVA) (seasons were shifted by 6 months in the Southern Hemisphere relative to their dates in the Northern Hemisphere).

Classifying the vertical patterns of slopes—The 410 vertical profiles of size distributions of particles were sorted into groups using a clustering technique. The Euclidean distance was computed between all pairs of profile slopes, and the flexible linkage hierarchical clustering method was used to classify the profiles (Lance and Williams 1967). The best number of clusters was determined using a new stopping rule, called the "random simulation test" (RST), which was developed for ecological data with strong variability (Guidi et al. 2009). The method generates a synthetic profile of slopes using values randomly chosen from a uniform distribution having the same mean and variance as the original data set for each 5-m depth interval, after which the new data set formed by adding the synthetic and actual data profiles is clustered. The clustering distance at which the synthetic profile forms a group by itself is chosen for cluster selection. By repeating the procedure 10,000 times, a frequency distribution of possible distances can be calculated. The distance with the highest frequency is used to select the groups.

Multivariate analysis: principal component regression—We integrated the particle-size distribution at 400 m and used the resulting value to compute the vertical flux at that depth (F_{400}) with Eq. 6. We then analyzed the relationship between variables in the euphotic zone and F_{400} using principal component regression. For this analysis, we used the mean values of three variables in the euphotic zone (i.e., f_{micro}, f_{nano}, and f_{pico}), and four variables vertically integrated down to Z_e, i.e., B_a and Chl a in each of the three phytoplankton size fractions (B_{micro}, B_{nano}, and B_{pico}). The independent variable of the regression was the log-transformed mass flux at 400 m (F_{400}). The MLD was not included in the principal component regression because it decreased the value of the correlation coefficient between the flux and the independent variables.

Classical multiple regression between a dependent variable Y and p independent variables X_j provides a forecasting model $\hat{Y} = X_0 + B_1X_1 + \cdots + B_pX_p$ and estimates of the contribution of each X_j to the variance of Y. However, the required conditions for its use (i.e., normality of Y and X_js, absence of collinearity among the X_js, and linear dependence of Y on the X_js) are difficult to meet in practice. As a result, the estimates of regression coefficients are often biased (Jolliffe 1986).

In order to avoid the problem of collinearity among the X_js, we used principal component regression (PCR; e.g., Legendre and Legendre 1998), which corresponds to a multiple regression between Y and a subset of x principal components (C_j) of matrix X, computed on the correlation matrix among the X_js. PCR has been used for meteorological forecasting and for reconstructing paleoclimates (Buckley et al. 2004). The principal components (PCs) are selected based on the values of their squared correlation coefficients with the dependent variable. The number of PCs to be retained is determined by finding the inflexion in the curve representing the cumulated sum of the squared correlation coefficients as the function of the number of PCs retained, i.e., at that point, the model accounts for most of the variability in the data. The normality of the residuals of the model ($\varepsilon = Y - \hat{Y}$) was tested considering the probabilities of the skewness and the kurtosis of their distribution.

Results

World-ocean size distributions of particles—The clustering process identified six different patterns in the vertical profiles of slopes (b) of the particle-size distributions (Fig. 2). Each cluster included data collected with at least two of the three UVP generations. The visual characteristics of size distributions of particles that most influenced the clustering of profiles appeared to be the changes of b with depth and the values of b in the mesopelagic layer (from 300 m down to 1000 m). All clusters had an abrupt change in b within the upper 300 m of the water column; below 300 m, b decreased with depth for cluster 5 (from -2 to -4), increased for cluster 4 (from -5 to -3.5), and was relatively constant for cluster 1, cluster 2, cluster 3, and cluster 6. The median b for all depths of the 410 profiles was about -4. A decrease in b with depth (e.g., from -3 to -4) means a downward increase in the proportion of small

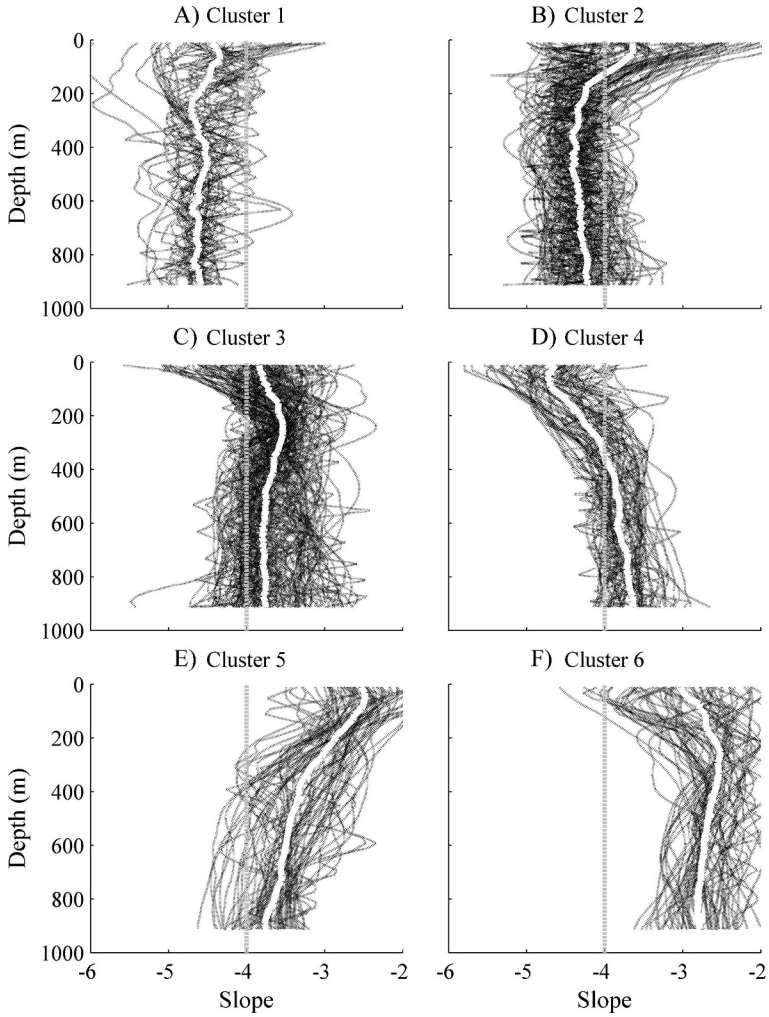

Fig. 2. Vertical profiles of the slopes of particle-size distributions, grouped into six clusters. Bold white lines: median profiles.

particles, whereas an increase in b with depth (e.g., from -5 to -4) means a downward decrease in the proportion of large particles.

The clusters differed in their values of b in the mesopelagic layer (Fig. 2). Vertical profiles from clusters 1 and 2 (25% of total) had $b < -4$ and were located predominantly in waters with low productivity at the season the profiles were recorded. These included the Mediterranean Sea and the Atlantic Ocean in late summer and autumn, the Indian Ocean off the western coast of Australia, and the South Pacific Gyre (Fig. 3).

Vertical profiles from cluster 6 (15% of total) had $b > -4$ and as large as -2 , and were mostly located in waters that were very productive at the time the profiles were recorded. Profiles from cluster 6 were located in upwelling zones along the Pacific coast of Chile and along the Atlantic coast of northwest Africa, in the Mediterranean Sea and the center of the North Atlantic in spring, and around Kerguelen Island in the Indian Sector of the Southern Ocean (Figs. 2, 3).

Most vertical profiles from cluster 3, cluster 4, and cluster 5 (which include 60% of the 410 profiles) were located in the North Atlantic Ocean. The other profiles from these three clusters were located around the highly productive Kerguelen Plateau, around the Marquesas Islands in the tropical South Pacific, in the minimum-oxygen zone off Chile in the Pacific Ocean, in the Mediterranean Sea, and off the western Australian coast (Fig. 3).

Table 3 gives the phytoplankton characteristics and calculated mass flux of particles for the six clusters. Clusters 1 to 4 had very low fractions of microphytoplankton (f_{micro} = 10–20%), and were co-dominated by nanoplankton and picophytoplankton ($f_{nano} + f_{pico}$ = 43%). The lowest integrated TChl a value (B_a) and mass flux at 400 m (F_{400}) were observed for cluster 1 (i.e., B_a = 6.9 mg m^{-2} and F_{400} = 3.3 mg m^{-2} d^{-1}). Cluster 4 was dominated by nanophytoplankton, with f_{nano} = 52%, f_{pico} = 32%, and f_{micro} = 16%; its TChl a was high (B_a = 28 mg m^{-2}), whereas its mass flux was low (F_{400} = 11.7 mg m^{-2} d^{-1}). The values of B_a were low, and the values of F_{400} were high for cluster 5 (i.e., 19.3 mg m^{-2} and 56.2 mg m^{-2} d^{-1}, respectively), which was dominated by nanophytoplankton (f_{nano} = 49%, f_{micro} = 27%, f_{pico} = 24%).

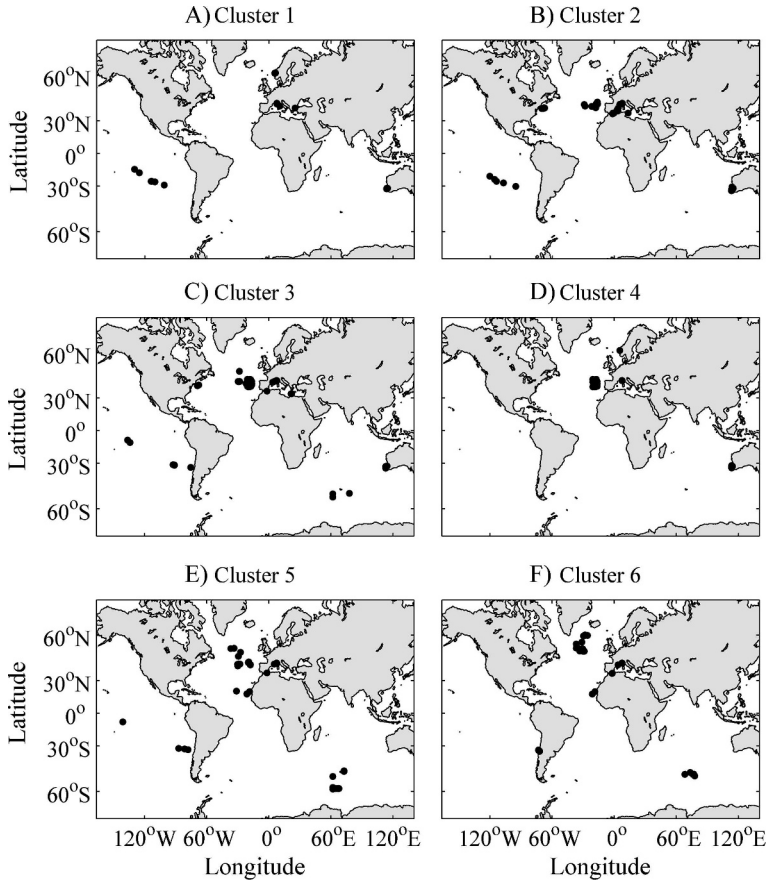

Fig. 3. Locations of the six clusters (black dots) of vertical profiles of particle-size distributions (Fig. 2) in the world ocean.

Cluster 6 was associated with productive waters and was dominated by microplankton (f_{micro} = 65%, f_{nano} = 16% and f_{pico} = 19%). Cluster 6 also had the highest B_a and F_{400} (i.e., 38.0 mg m^{-2} and 315 mg m^{-2} d^{-1}, respectively).

Mass flux and phytoplankton community structure—Flux estimates at 400 m computed with Eq. 6 ranged between 1.8 mg m^{-2} d^{-1} and 578 mg m^{-2} d^{-1}. B_a and F_{400} were significantly correlated (Spearman's r = 0.50, $p < 0.001$). The highest mass fluxes (F_{400} > 100 mg m^{-2} d^{-1}) were associated with profiles dominated by microphytoplankton in the euphotic zone (f_{micro} > 60%; Fig. 4A). The lowest fluxes were associated with surface communities with the smallest observed B_a and dominated by picophytoplankton (f_{pico} > 40%; Fig. 4C). Mass fluxes had intermediate values when phytoplankton structure was dominated by nanophytoplankton (f_{nano} > 50%; Fig. 4B).

The previous results are summarized in a ternary plot displaying together f_{micro}, f_{nano}, f_{pico} and F_{400} (Fig. 5A). This representation shows that high F_{400} (>100 mg m^{-2} d^{-1}) were associated with dominance by microphytoplankton (f_{micro} > 60%) in the euphotic zone, and low F_{400} (<10 mg m^{-2} d^{-1}) were associated with dominance by either nanophytoplankton (f_{nano} > 50%) or picophyto-

Table 3. For the 6 clusters, phytoplankton size structure (f_{micro}, f_{nano}, and f_{pico} as % of total phytoplankton), integrated Chl *a* (B_a) in the euphotic zone, total mass flux of particles at 400 m (F_{400}), and depth of the surface mixed layer (MLD). Mean values and standard deviations (SD).

	f_{micro} (%)		f_{nano} (%)		f_{pico} (%)		Euphotic-zone Chl *a* (mg m^{-2})		F_{400} (mg m^{-2} d^{-1})		MLD (m)	
Clusters	Mean	SD	Mean	SD	Mean	SD	Mean	SD	Mean	SD	Mean	SD
1	10	3	35	6	55	8	6.9	2.9	3.3	1.4	16.9	11.5
2	20	9	47	8	33	16	20.0	10.3	40.2	77.7	21.8	18.8
3	14	9	48	12	38	17	22.0	8.0	22.8	49.5	34.7	34.5
4	16	10	52	11	32	13	28.0	5.9	11.7	5.9	45.4	43.8
5	27	16	49	8	24	14	19.3	6.9	56.2	61.6	42.3	38.5
6	65	19	16	12	19	18	38.0	12.7	315.0	176.0	22.3	10.7

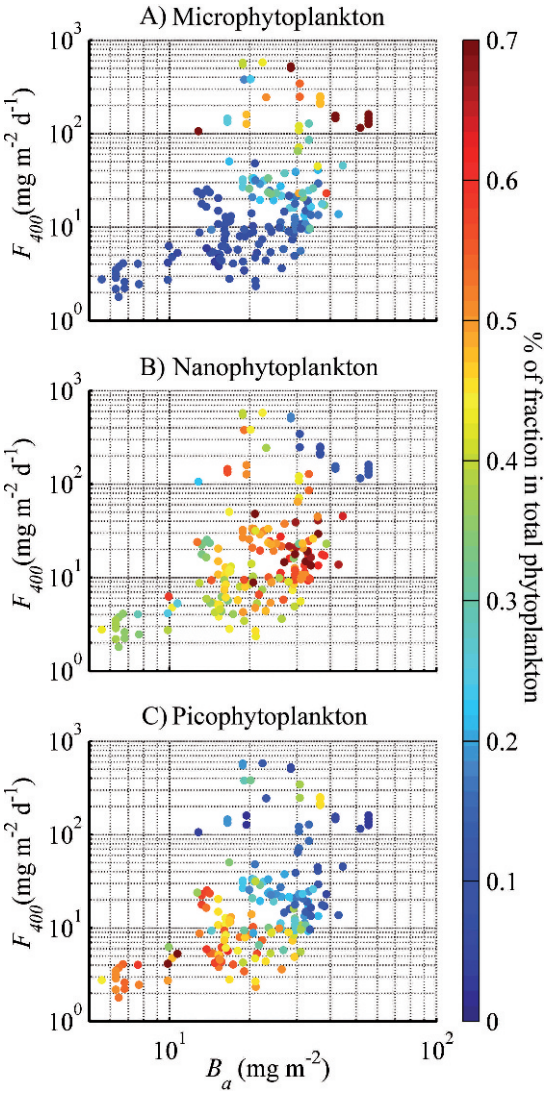

Fig. 4. Relative abundance (indicated by the color of dots) of phytoplankton in the three size fractions (f_{micro}, f_{nano}, and f_{pico}) represented as a function of integrated chlorophyll *a* in the euphotic zone (B_a) and the estimated flux at 400 m.

plankton ($f_{pico} > 40\%$). F_{400} increased with B_a when f_{micro} increased and f_{nano} and f_{pico} decreased (Figs. 4, 5A). Values of coefficient k of the Martin power relationship (Eq. 8) varied between 0.2 and 1.0 (Fig. 5B). Possible seasonality of k was tested using the Kruskal-Wallis nonparametric one-way ANOVA. The medians of 125 profiles from spring, 5 from summer, 14 from autumn, and 49 from winter ($k = 0.37$) were $k = 0.52$, $k = 0.47$, $k = 0.47$ and $k = 0.37$, respectively. Overall, there were significant differences in k among seasons (Kruskal-Wallis test, $p < 0.001$).

Principal component regression (PCR) analysis showed that only component 1, component 4, and component 2 (in that order) were strongly correlated with F_{400} (Table 4; $p < 0.01$); R^2 did not increase significantly when including other components in the regression ($p > 0.01$). Hence, only component 1, component 4, and component 2 were used for the multiple regression analysis. The resulting model explains 68% of the variance of F_{400}:

$$\ln(F_{400}) = -0.48C_1 + 1.45C_4 + 0.19C_2 + 2.85 \quad (9)$$

The regression coefficients and their confidence intervals are given in rightmost three columns of Table 4.

Because principal components are linear combinations of the original variables with their corresponding eigenvectors, we could transform Eq. 9 to express the regression model in term of the original variables (Legendre and Legendre 1998, their Eq. 10.17):

$$\ln(F_{400}) = -5.73f_{pico} + 5.17f_{micro} + 0.15B_{pico} - 0.04B_{micro} - 0.02B_a - 0.02B_{nano} - 0.46f_{nano} + 3.98 \quad (10)$$

The distribution of residuals was tested against a normal distribution. Skewness was equal to 0.25 ($p = 0.08$), and kurtosis was equal to 0.07 ($p = 0.42$), indicating that the distribution of residuals was not significantly different from a normal distribution ($p > 0.05$).

Eq. 10 was used to estimate the mass flux at 400 m (F_{400}), and resulting values were compared to the flux estimated from the size distribution of particles at the same depth (Eq. 6). The correspondence between the two sets of values was good (Fig. 6; $r^2 = 0.68$ and $p < 0.01$).

Finally, f_{micro} and f_{pico} were significantly correlated to k (Spearman $r = -0.49$ and 0.40, respectively; $p < 0.001$). The linear relationship between k and these two phytoplankton fractions was significant ($R^2 = 0.28$, $F = 37.2$, $p < 0.001$), but that multiple relationship was not significantly better than the simple regression of k on f_{pico} only ($R^2 = 0.27$). Hence,

$$k = 0.80 - 0.89f_{pico} \quad (11)$$

Discussion

Size of particles and phytoplankton community structure—Large phytoplankton cells in the euphotic zone, such as chain-forming diatoms, have been associated with the occurrence of large aggregates on the sea floor after bloom events (Beaulieu 2002). Regional studies in the Mediterranean Sea and the North Atlantic have shown a correlation between microphytoplankton abundance and the size of particles in the upper 1000 m of the water column (Stemmann et al. 2002; Guidi et al. 2007). In the present study, we focused on global trends in the relationships between the size of particles, their vertical export, and the phytoplankton community independently from the time or location of studies. This type of analysis had not been done previously, partly because global data were unavailable until recently. Our clustering analysis on the particle-size distributions partitioned the world-ocean vertical profiles into six groups. The resulting clusters were closely associated with different phytoplankton communities in the euphotic zone, and those communities influenced more F_{400} than B_a (Fig. 4, Table 3). The clustering analysis identified two extreme situations and several intermediate ones (Fig. 2). The slopes of the size distributions of particles were <-4 at low B_a (6.9 mg m^{-2} $\pm$ 2.9) when

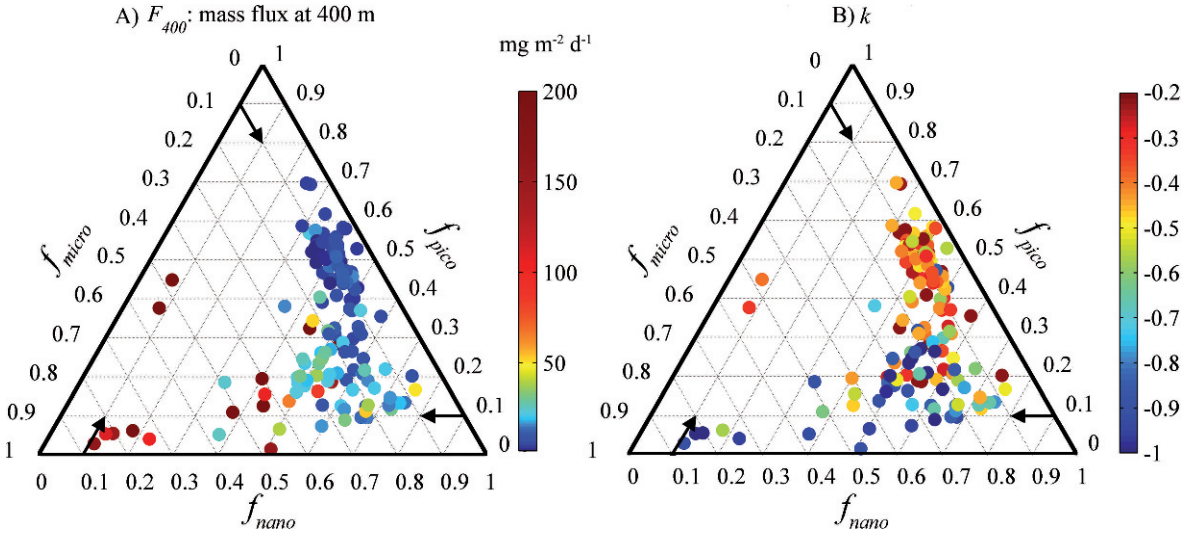

Fig. 5. Ternary plots of the flux of particles in the mesopelagic layer. (A) Total flux of particles at 400 m (F_{400}; color of dots) plotted as a function of phytoplankton in the three size fractions. (B) Exponent of the Martin power relationship (k; Eq. 8) fitted to the flux data (color of dots) and plotted as a function of phytoplankton in three size fractions. Mass-flux profiles were calculated from the size distributions of particles (Eq. 6). The arrows indicate how to read the values on the axes, the base referring to the axis and the head to the direction of reading.

or where picophytoplankton dominated the phytoplankton assemblage (cluster 1; Figs. 2, 3). Dominance by picoplankton and low biomass are typical of oligotrophic waters (Partensky et al. 1999). At the other end of the range, cluster 6 was characterized by large particles ($b > -4$) associated with high B_a (38 mg m^{-2} ± 12.7) and dominance of microphytoplankton. Clusters 2 to 5 corresponded to intermediate situations where the euphotic zone was dominated by medium-sized cells (nanophytoplankton).

Our study shows that b varies over a wide range in oceans (i.e., from −5 to −2), which goes against the idea that the slope of the particle-size spectrum is −4 (Sheldon et al. 1972). This has consequences on all studies that refer to the size distribution of particles, including the estimation of downward POC fluxes from Thorium 234/Uranium 238 (^{234}Th/^{238}U) disequilibrium where the particle-size distribution must be considered (Burd et al. 2007).

Vertical patterns in the size of particles: physical and biological controls—The values of b and their vertical changes provide insights into the processes that affect particle dynamics and fate. There are several physical and biological processes that consume and redistribute the organic matter contained in sinking aggregates. Some biological processes, such as microbial degradation (Ploug and Grossart 2000) and zooplankton fragmentation (Goldthwait et al. 2004), and some physical processes, such as disaggregation from turbulence (MacIntyre et al. 1995), could decrease the median size of aggregates and therefore reduce the related carbon flux to the deep ocean when particle consumption occurs simultaneously. Conversely, other physical processes (e.g., coagulation; Jackson 1990) and biological processes (e.g., zooplankton grazing; Graham et al. 2000; Stemmann et al. 2004) could increase the median size of aggregates and therefore contribute to increase the carbon flux to the deep ocean.

Table 4. Components of the PCR sorted by decreasing correlation with F_{400}, and corresponding r^2, R^2 (cumulated sum of r^2), and associated probability (p). The three components selected for the PCR are in bold. For component 1, component 4, and component 2, coefficients of the multiple regression model and their 5% confidence intervals based on the components of PCR.

Components	Correlation with F_{400} (r)	r^2	R^2	Associated p	Regression coefficients	Confidence interval	
1	−0.67	0.45	0.45	<0.01	−0.48	−0.54	−0.42
4	0.43	0.18	0.63	<0.01	1.45	1.17	1.73
2	0.22	0.05	0.68	<0.01	0.19	0.12	0.26
3	−0.08	0.007	0.68	0.26			
5	−0.05	0.002	0.68	0.53			
6	−0.04	0.002	0.68	0.56			
7	−0.03	0.0009	0.69	0.68			
y-intercept					2.85	2.74	2.95

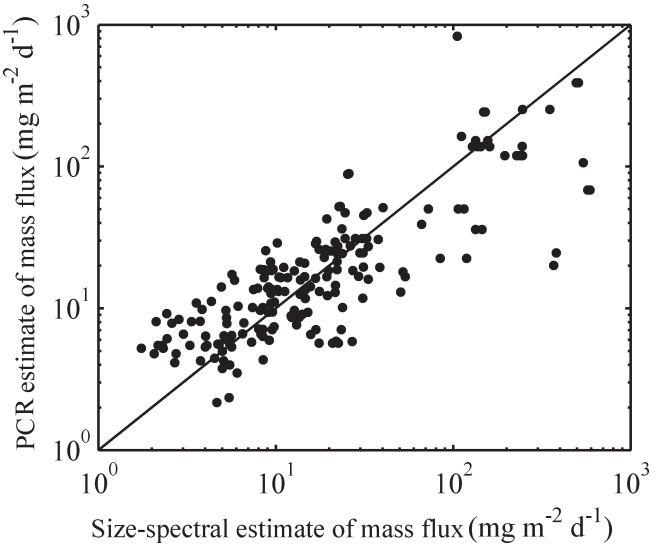

Fig. 6. Flux of particles estimated at 400 m using the size distribution of particles (Eq. 6) vs. values modeled by PCR (Eq. 9); $n = 193$, $r^2 = 0.68$, and $p < 0.01$. The 1 : 1 line is provided as visual reference.

Interactions among the above processes are complex and remain unclear. Particle mass flux is the product of particle concentration, sinking speed, and mass. The only process that decreases the flux is consumption; all other processes only shift particle mass and flux to different size intervals (Jackson and Burd 2002). Recent studies have shown that the average size of particles decreases with depth, suggesting that fragmentation processes could be dominant (Stemmann et al. 2004). However, other studies have shown that the average sinking speed increases with depth, suggesting that the size could increase (Gehlen et al. 2006) or that aggregates become denser as they sink (Berelson 2002).

In the present work, we conducted a systematic analysis of the vertical patterns in sizes of particles ranging from 250 μm to 1.5 mm, over a wide range of ocean conditions. There was little change with depth in b for cluster 1 (27 vertical profiles). The available data do not provide enough information to decide whether the vertical homogeneity of profiles resulted from low aggregation or dispersion processes, or from mutual compensation of these processes during the downward transit of particles. The fact that these profiles were all from oligotrophic regions suggests that processes there occurred at low rates. The other five clusters (i.e., clusters 2 to 6) showed large changes of b within the upper 300 m of the water column. This implies that the upper 300 m of the water column were the site of intense biological and physical processes that transformed the size distributions of particles and thus modified the flux of particles to the mesopelagic layer. Below 300 m, most of the clusters showed a decrease in b, implying a reduction of the median size of particles as depth increased. Hence, the mechanisms that drive the fragmentation and consumption of particles in the mesopelagic layer should be central to the modeling of deep vertical particle fluxes. Only cluster 4 showed an increase in the median size of particles within the mesopelagic layer. This cluster consisted of profiles recorded in the northeastern Atlantic during Aug–Sep 2001. Guidi et al. (2007) proposed that the observed increase with depth in particle concentration and size was the signature of the spring-bloom enrichment in particles that sank down slowly and were seen at depths >500 m in late summer. As proposed by Stemmann et al. (2004), the use of time series of size distributions of particles combined with the modeling of processes that change the size distribution of particles as they sink would significantly improve the description and analysis of the decay of the downward particle flux in oceans. In any case, combined water-column data on phytoplankton, heterotrophic bacteria, zooplankton, and sinking particles are needed to model the forcing of the particle flux by the food web. Because such data are not available on a global scale, we could not develop this type of model in the context of the present work.

Coupling between phytoplankton community structure, size of particles, and vertical export—The fate of particulate production exported to the mesopelagic layer is generally modeled using empirical power relationships with an exponent k that describes the decrease in vertical flux as a function of depth (Suess 1980; Martin et al. 1987; this study, Eq. 8). With the exception of a few syntheses (Lutz et al. 2002; Dunne et al. 2005), many quantitative biogeochemical studies used the parameterization of the Martin power relationship with a single value for exponent k (Eq. 8). However, it is known that the rate of decrease of the particulate flux with depth varies within and among ocean basins (Karl et al. 1996; Usbeck et al. 2003; Buesseler et al. 2007). Furthermore, k has been correlated with phytoplankton biomass and primary production (Boyd and Trull 2007). Results tend to show that the downward decrease in flux increases with increased phytoplankton biomass or primary production (Berelson 2002).

The estimates of k in the literature are based on sediment-trap data, which are scarce both horizontally and vertically. The scarcity of flux data results in high uncertainty in the estimates of k, which precludes regionalization (Primeau 2006). Using our extensive data set, which covers all trophic regimes in the world ocean and has a vertical resolution of 5 m, we could address problems such as spatial variability in k. Our data show that both the flux at a 400-m depth (Fig. 5A) and the rate of change of the vertical flux with depth (Fig. 5B) vary as a function of the phytoplankton assemblage in the euphotic zone. Our results indicate that there are at least two patterns in the dynamics of particles (Figs. 2, 3). In the first pattern, aggregates formed in surface waters dominated by microphytoplankton, leading to high mass flux at 400 m, with a sharp decrease in flux (i.e., strong remineralization) between 100 m and 300 m. This resulted in a high value of k (>0.8, Fig. 5B). The second pattern occurred in oligotrophic waters dominated by picophytoplankton with lower mass flux at 400 m, which represented not more than 20% of the flux at Z_e. Hence, a low value of k (<0.3, Fig. 5B).

We found that there was a significant effect of season on k. The highest values of k (median = 0.52) were calculated

during spring, i.e., the season with diatom blooms in the North Atlantic and in the Mediterranean Sea (Smetacek 1985). At the global scale, however, diatoms are dominant during wintertime, this trend being driven by the Southern Ocean (Alvain et al. 2008). At the opposite end of the spectrum, the lowest values of k (median = 0.37) were calculated during winter, i.e., the season dominated by small cells when excluding the Southern Ocean (Alvain et al. 2008). Hence, there may not have been a significant seasonal difference among k values if our data set had included winter particle profiles from the Southern Ocean. It follows that phytoplankton structure may be a more important determinant of export than season.

The two patterns discussed above suggest that in eutrophic waters during a phytoplankton bloom, there is rapid sinking of large phytoplankton aggregates formed by coagulation or produced by zooplankton. The vertical flux mediated by these sinking particles is reduced by processes such as copepod coprehexy and coprophagy on fecal pellets (Lampitt et al. 1990; Wassmann et al. 2000) or copepod grazing on particles (Kiørboe 2000). Such processes could cause a significant reduction of the flux with depth (Stemmann et al. 2004; Steinberg et al. 2008). However, a non-negligible fraction of large particles escape destruction by zooplankton processes in the euphotic zone and sink to the mesopelagic layer, which results in a higher mass flux than in systems dominated by picophytoplankton.

In oligotrophic waters, particles are smaller than in more productive waters, resulting in low sinking speeds and particle transformations being dominated by bacterial degradation (Karl et al. 1988). The small size of phytoplankton and steady remineralization pressure prevent the accumulation of large particles in the euphotic zone. When this situation lasts for a long period, small particles are produced and remineralized at constant rates (Fig. 5A, B). Furthermore, it is possible that particles in oligotrophic conditions contain more refractory organic or mineral matter than in eutrophic conditions, which would prevent fast remineralization of the settling material and thus promote microbial degradation vs. zooplankton consumption and conserve the size distribution with depth. More data on chemical composition of particles need to be collected in order to test this hypothesis.

Using Eqs. 9 and 10, we found that phytoplankton composition in the euphotic zone explained 68% of the variance of the downward flux at 400 m. We also found (Fig. 6) that the flux values from Eq. 10 corresponded well to values estimated from the size distribution of particles at the same depth (Eq. 6). Hence, the results of statistical analyses were consistent with our above explanation that the downward flux of particles was influenced by food-web processes linked to the structure of the phytoplankton community in the euphotic zone.

In this study, we showed that the size distributions of particles and estimated flux at 400 m were related to the composition of the phytoplankton assemblage in the euphotic zone. It follows that systems dominated by picoplankton and microphytoplankton should be represented in biogeochemical models by different values of k in the Martin power relationship (Fig. 7), i.e., high k values in

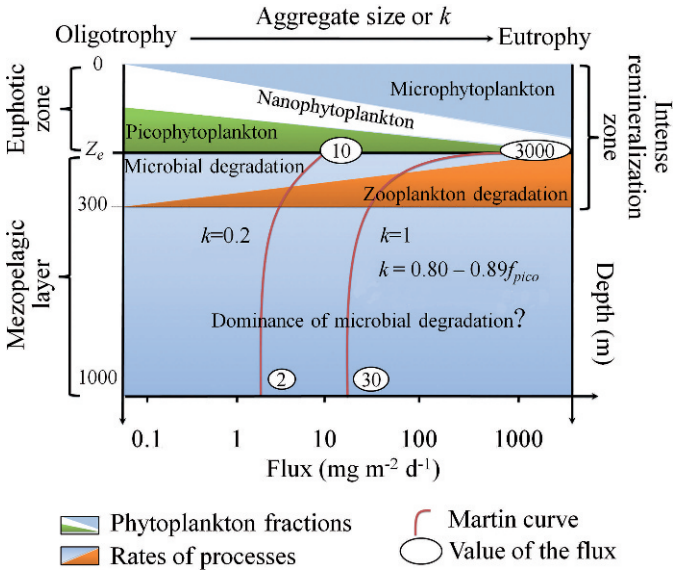

Fig. 7. Schematic representation of different processes that can affect the size distribution and decrease in the flux of particles in oceans. The width of the different surfaces in the zone of intense remineralization represents the relative importance of phytoplankton fractions or processes rates, and k is the value of the exponent of the Martin power relationship (Eq. 8). The equation to calculate k from the size structure of phytoplankton corresponds to Eq. 11 in the text.

systems dominated by microphytoplankton in the euphotic zone and low k values in systems dominated by picophytoplankton. In the Results section, we presented a relationship between k and f_{pico} (Eq. 11) that can be used to predict or constrain the decrease of the particle export with depth based on phytoplankton composition in the euphotic zone. Even if the relationship in Eq. 11 is significant, it represents only 27% of the variability of k. This relatively low R^2 reflects the complexity of the interactions between the formation of particles in the euphotic zone, their downward export, and their transformation during their transit to depth. Nevertheless, biogeochemists and modellers could use Eq. 11 to obtain a realistic description of the downward particle flux instead of using a constant k value as if often done. With Eq. 11, it would be possible to take into account regional and temporal differences in food-web effects on downward carbon fluxes, and thus improve the quantification of the biological pump at the global scale.

Acknowledgments

The authors thank the officers and crews of the many vessels used in this study for their assistance and support. The authors also thank two anonymous reviewers who provided excellent suggestions.

L. Guidi received financial support from the French Ministère de l'Education Nationale, de l'Enseignement Supérieur et de la Recherche, from the European Commission's Sixth Framework Programme under the priority 'Sustainable Development Contract GOCE-2006-036949,' and from the Gordon and Betty Moore Foundation and C–MORE. G. Jackson received support from National Science Foundation grants OCE-0352127 and OCE-0327644. The data were acquired on several cruises

(Table 1) funded by the Joint Global Ocean Flux Study-France (JGOFS), Biogeochemical processes in the Ocean and Fluxes (PROOF), and Cycles Biogéochimiques, Environnement et Ressources (LEFE-CYBER) programs.

References

Alldredge, A. L., and M. W. Silver. 1988. Characteristics, dynamics, and significance of marine snow. Prog. Oceanogr. **20:** 41–82.

Alvain, S., C. Moulin, Y. Dandonneau, and H. Loisel. 2008. Seasonal distribution and succession of dominant phytoplankton groups in the global ocean: A satellite view. Glob. Biogeochem. Cyc. **22:** GB3001, doi: 10.1029/2007GB003154.

Armstrong, R. A., C. Lee, J. I. Hedges, S. Honjo, and S. G. Wakeham. 2002. A new, mechanistic model for organic carbon fluxes in the ocean based on the quantitative association of POC with ballast minerals. Deep-Sea Res. II **49:** 219–236.

Beaulieu, S. E. 2002. Accumulation and fate of phytodetritus on the sea floor. Oceanogr. Mar. Biol. **40:** 171–232.

Berelson, W. M. 2002. Particle settling rates increase with depth in the ocean. Deep-Sea Res. II **49:** 237–251.

Boyd, P. W., and P. P. Newton. 1999. Does planktonic community structure determine downward particulate organic carbon flux in different oceanic provinces? Deep-Sea Res. I **46:** 63–91.

———, and T. W. Trull. 2007. Understanding the export of biogenic particles in oceanic waters: Is there consensus? Prog. Oceanogr. **72:** 276–312.

Buckley, B. M., R. J. S. Wilson, P. E. Kelly, D. W. Larson, and E. R. Cook. 2004. Inferred summer precipitation for southern Ontario back to AD 610, as reconstructed from ring widths of *Thuja occidentalis*. Can. J. For. Res. **34:** 2541–2553.

Buesseler, K. O., and others. 2007. An assessment of the use of sediment traps for estimating upper ocean particle fluxes. J. Mar. Res. **65:** 345–416.

Burd, A. B., G. A. Jackson, and S. B. Moran. 2007. The role of the particle size spectrum in estimating POC fluxes from $^{234}Th/^{238}U$ disequilibrium. Deep-Sea Res. I **54:** 897–918.

Claustre, H. 1994. The trophic status of various oceanic provinces as revealed by phytoplankton pigment signatures. Limnol. Oceanogr. **39:** 1206–1210.

Dunne, J. P., R. A. Armstrong, A. Gnanadesikan, and J. L. Sarmiento. 2005. Empirical and mechanistic models for the particle export ratio. Glob. Biogeochem. Cyc. **19:** GB4026, doi: 10.1029/2004GB002390.

Eppley, R. W., and B. J. Peterson. 1979. Particulate organic-matter flux and planktonic new production in the deep ocean. Nature **282:** 677–680.

Gehlen, M., L. Bopp, N. Ernprin, O. Aumont, C. Heinze, and O. Raguencau. 2006. Reconciling surface ocean productivity, export fluxes and sediment composition in a global biogeochemical ocean model. Biogeosciences **3:** 521–537.

Goldthwait, S., J. Yen, J. Brown, and A. Alldredge. 2004. Quantification of marine snow fragmentation by swimming euphausiids. Limnol. Oceanogr. **49:** 940–952.

Gorsky, G., M. J. Chretiennot-Dinet, J. Blanchot, and I. Palazzoli. 1999. Picoplankton and nanoplankton aggregation by appendicularians: Fecal pellet contents of *Megalocercus huxleyi* in the equatorial Pacific. J. Geophys. Res-Oceans. **104:** 3381–3390.

———, M. Picheral, and L. Stemmann. 2000. Use of the underwater video profiler for the study of aggregate dynamics in the North Mediterranean. Estuar. Coast. Shelf Sci. **50:** 121–128.

Graham, W. M., S. Macintyre, and A. L. Alldredge. 2000. Diel variations of marine snow concentration in surface waters and implications for particle flux in the sea. Deep-Sea Res. I **47:** 367–395.

Guidi, L., G. A. Jackson, L. Stemmann, J. C. Miquel, M. Picheral, and G. Gorsky. 2008. Relationship between particle size distribution and flux in the mesopelagic zone. Deep-Sea Res. I **55:** 1364–1374.

———, F. Ibanez, V. Calcagno, and G. Beaugrand. 2009. A new procedure to optimize the selection of groups in a classification tree: Applications for ecological data. Ecol. Model. **220:** 451–461.

———, L. Stemmann, L. Legendre, M. Picheral, L. Prieur, and G. Gorsky. 2007. Vertical distribution of aggregates (>110 μm) and mesoscale activity in the northeastern Atlantic: Effects on the deep vertical export of surface carbon. Limnol. Oceanogr. **52:** 7–18.

Ibanez, F., and M. Etienne. 1992. Filtering of temporal series by principal component analysis of processes (PCAP). J. Rech. Océanogr. **16:** 27–33.

Jackson, G. A. 1990. A model of the formation of marine algal flocs by physical coagulation processes. Deep-Sea Res. **37:** 1197–1211.

———, and A. B. Burd. 2002. A model for the distribution of particle flux in the mid-water column controlled by subsurface biotic interactions. Deep-Sea Res. II **49:** 193–217.

———, R. Maffione, D. K. Costello, A. L. Alldredge, B. E. Logan, and H. G. Dam. 1997. Particle size spectra between 1 μm and 1 cm at Monterey Bay determined using multiple instruments. Deep-Sea Res. I **44:** 1739–1767.

Jolliffe, I. T. 1986. Principal component analysis. Springer Verlag.

Karl, D. M., J. R. Christian, J. E. Dore, D. V. Hebel, R. M. Letelier, L. M. Tupas, and C. D. Winn. 1996. Seasonal and interannual variability in primary production and particle flux at station ALOHA. Deep-Sea Res. II **43:** 539–568.

———, G. A. Knauer, and J. H. Martin. 1988. Downward flux of particulate organic matter in the ocean—a particle decomposition paradox. Nature **332:** 438–441.

Kiørboe, T. 2000. Colonization of marine snow aggregates by invertebrate zooplankton: Abundance, scaling, and possible role. Limnol. Oceanogr. **45:** 479–484.

Lampitt, R. S., T. Noji, and B. Bodungen. 1990. What happens to zooplankton faecal pellets? Implications for material flux. Mar. Biol. **104:** 15–23.

Lance, G. N., and W. T. Williams. 1967. A general theory of classificatory sorting strategies. 1. Hierarchical systems. Comput. J. **9:** 373–380.

Legendre, P., and L. Legendre. 1998. Numerical ecology, 2nd English ed. Elsevier.

Lutz, M., R. Dunbar, and K. Caldeira. 2002. Regional variability in the vertical flux of particulate organic carbon in the ocean interior. Glob. Biogeochem. Cyc. **16:** 1037, doi: 10.1029/2000GB001383.

MacIntyre, S., A. L. Alldredge, and C. C. Gotschalk. 1995. Accumulation of marine snow at density discontinuities in the water column. Limnol. Oceanogr. **40:** 449–468.

Mantoura, R. F. C., and C. A. Llewellyn. 1983. The rapid-determination of algal chlorophyll and carotenoid pigments and their breakdown products in natural waters by reverse-phase high-performance liquid chromatography. Anal. Chim. Acta **151:** 297–314.

Martin, J. H., G. A. Knauer, D. M. Karl, and W. W. Broenkow. 1987. Vertex: Carbon cycling in the northeast Pacific. Deep-Sea Res. **34:** 267–285.

McCave, I. N. 1984. Size spectra and aggregation of suspended particles in the deep ocean. Deep-Sea Res. **31:** 329–352.

Michaels, A. F., and M. W. Silver. 1988. Primary production, sinking fluxes, and the microbial food web. Deep-Sea Res. **35:** 473–490.

Morel, A., and J. F. Berthon. 1989. Surface pigments, algal biomass profiles, and potential production of the euphotic layer: Relationships reinvestigated in view of remote-sensing applications. Limnol. Oceanogr. **34:** 1545–1562.

———, and S. Maritorena. 2001. Bio-optical properties of oceanic waters: A reappraisal. J. Geophys. Res.-Oceans. **106:** 7163–7180.

Olli, K., and others. 2007. The fate of production in the central Arctic Ocean—top-down regulation by zooplankton expatriates? Prog. Oceanogr. **72:** 84–113.

Partensky, F., W. R. Hess, and D. Vaulot. 1999. *Prochlorococcus*, a marine photosynthetic prokaryote of global significance. Microbiol. Mol. Biol. R. **63:** 106–127.

Peterson, M. L., S. G. Wakeham, C. Lee, M. A. Askea, and J. C. Miquel. 2005. Novel techniques for collection of sinking particles in the ocean and determining their settling rates. Limnol. Oceanogr.-Meth. **3:** 520–532.

Ploug, H., and H. P. Grossart. 2000. Bacterial growth and grazing on diatom aggregates: Respiratory carbon turnover as a function of aggregate size and sinking velocity. Limnol. Oceanogr. **45:** 1467–1475.

Primeau, F. 2006. On the variability of the exponent in the power law depth dependence of POC flux estimated from sediment traps. Deep-Sea Res. I **53:** 1335–1343.

Ras, J., H. Claustre, and J. Uitz. 2008. Spatial variability of phytoplankton pigment distributions in the subtropical South Pacific Ocean: Comparison between in situ and predicted data. Biogeosciences **5:** 353–369.

Richardson, T. L., and G. A. Jackson. 2007. Small phytoplankton and carbon export from the surface ocean. Science **315:** 838–840.

Sheldon, R. W., A. Prakash, and W. H. Sutcliff. 1972. Size distribution of particles in ocean. Limnol. Oceanogr. **17:** 327–340.

Smetacek, V. S. 1985. Role of sinking in diatom life-history cycles: Ecological, evolutionary, and geological significance. Mar. Biol. **84:** 239–251.

Steinberg, D. K., B. A. S. Van Mooy, K. O. Buesseler, P. W. Boyd, T. Kobari, and D. M. Karl. 2008. Bacterial vs. zooplankton control of sinking particle flux in the ocean's twilight zone. Limnol. Oceanogr. **53:** 1327–1338.

Stemmann, L., G. Gorsky, J. C. Marty, M. Picheral, and J. C. Miquel. 2002. Four-year study of large-particle vertical distribution (0–1000 m) in the NW Mediterranean in relation to hydrology, phytoplankton, and vertical flux. Deep-Sea Res. II **49:** 2143–2162.

———, G. A. Jackson, and G. Gorsky. 2004. A vertical model of particle size distributions and fluxes in the midwater column that includes biological and physical processes—part II: Application to a three-year survey in the NW Mediterranean Sea. Deep-Sea Res. I **51:** 885–908.

———, and others. 2008. Global zoogeography of fragile macrozooplankton in the upper 100–1000 m inferred from the Underwater Video Profiler. ICES J. Mar. Sci. **65:** 433–442.

Suess, E. 1980. Particulate organic-carbon flux in the oceans—surface productivity and oxygen utilization. Nature **288:** 260–263.

Uitz, J., H. Claustre, A. Morel, and S. B. Hooker. 2006. Vertical distribution of phytoplankton communities in open ocean: An assessment based on surface chlorophyll. J. Geophys. Res.-Oceans. **111:** C08005, doi: 10.1029/2005JC003207.

Usbeck, R., R. Schlitzer, G. Fischer, and G. Wefer. 2003. Particle fluxes in the ocean: Comparison of sediment trap data with results from inverse modeling. J. Mar. Syst. **39:** 167–183.

Vautard, R., and M. Ghil. 1989. Singular spectrum analysis in nonlinear dynamics, with applications to paleoclimatic time series. Physica D. **35:** 395–424.

Vidussi, F., H. Claustre, J. Bustillos-Guzman, C. Cailliau, and J. C. Marty. 1996. Determination of chlorophylls and carotenoids of marine phytoplankton: Separation of chlorophyll a from divinyl-chlorophyll *a* and zeaxanthin from lutein. J. Plankton Res. **18:** 2377–2382.

Wassmann, P., J. E. Ypma, and A. Tselepides. 2000. Vertical flux of faecal pellets and microplankton on the shelf of the oligotrophic Cretan Sea (NE Mediterranean Sea). Prog. Oceanogr. **46:** 241–258.

Associate editor: Mary I. Scranton

Received: 02 December 2008
Accepted: 14 June 2009
Amended: 25 June 2009